The influence of channel walls on flag flutter

Olivier Doaré, Christophe Eloy

THE INFLUENCE OF CHANNEL WALLS ON FLAG FLUTTER

Olivier Doaré[*]
Unité de Mécanique (UME), ENSTA-Paristech
Chemin de la Hunière,
91761, Palaiseau, FRANCE
Email: olivier.doare@ensta-paristech.fr
[*]Address all correspondence to this author

Chistophe Eloy
IRPHE, Université d'Aix-Marseille
49 rue Joliot-Curie,
13013, Marseille, France
Email: eloy@irphe.univ-mrs.fr

ABSTRACT

The effect of confinement of a rectangular channel on the flag flutter instability is investigated, both in terms of waves propagating in the infinite medium (local approach) and in terms of modes in the finite length system (global approach). Using a 1D Euler-Bernoulli model for the plate and a 3D potential flow model for the flow, the problem is solved numerically for various sets of the geometrical parameters to compute the critical velocity for instability as function of the mass ratio. It is found that the proximity of walls parallel and perpendicular the plate affects significantly the plate's dynamics and instability. One main conclusion of this work is that models considering a 2D flow can predict correctly the critical velocity only in specific cases such as large mass ratio, large aspect ratio or very confined plates.

INTRODUCTION

The equilibrium state of a cantilevered plate in an axial flow can become unstable once a critical value of the flow velocity is reached, resulting in oscillations of large amplitude. This phenomenon, referred to as *flag flutter* has been the focus of a large amount of researches, as reported in some recent books and reviews [1, 2]. Among the various linear models that atempted to give a numerical prediction of the critical flow velocity for apparition of flutter instability, one can distinguish three main families. In the first one, a 2D problem is considered, *i.e.* an infinite span plate in a 2D potential flow [3–5]. The approximation done in these models is referred to as *large span* approximation. In the second familiy, the typical wavelengths of deformation are considered large enough when compared to the typical size of the cross section of the plate, so that the perturbation of the flow at a given cross section depends only on the plate dynamics at this cross section [6]. These models are referred to as *slender body* models. The third family concerns models that do not consider any of the above approximations, and solve the 3D flow around the plate. This kind of model has shown that there is a strong influence on the aspect ratio of the plate on the critical velocity [7]. Works using similar method followed to study the presence of walls perpendicular to the plate (spanwise confinement) and showed that the critical velocity tends slowly to that predicted by a 2D model when the walls are approched [8]. In the present work, two additional walls, parallel to the plate are considered so that the latter is confined in a rectangular channel flow. The method used in the present paper is the same as developped in previous works [7, 8].

Experimentally, flag flutter has also been intensively investigated. The first experimental studies of the phenomenon are reported in references [3, 9, 10], among others. A consistent review of all experimental studies before 2004 can be found in reference [1]. These studies have shown that although the plate's dynamics is always two-dimensional, the values of the critical velocity predicted by 2D models are always lower than that found experimentally. Comparison with 3D models taking into account the finite aspect ratio of the plate significantly improved the prediction of the critical velocity [7] and a nonlinear model taking into account the initial spanwise curvature [11] explained the origin of the hysteresis observed experimentally. Finally, the effect of walls perpendicular to the plate has been investigated experimentally in reference [12] and results are in good agreement with the model developed in [8].

The paper is organized as follows. In the next section, the problem of a flat plate in a rectangular channel potential flow is formulated. The stability properties of the infinite length problem are then analysed. Next, a finite length system is considered.
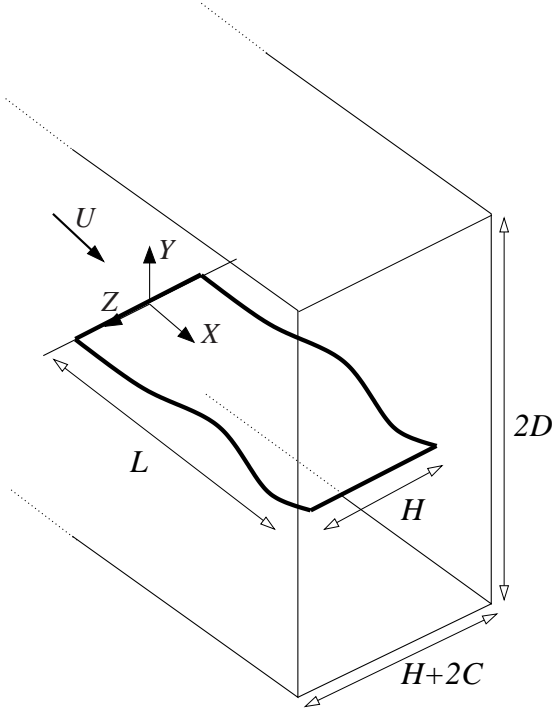
FIGURE 1: Skematic view of a plate in a rectangular channel.

1 FORMULATION OF THE PROBLEM
1.1 Coupled fluid-structure equations
The problem considered in this paper is sketched on Fig. 1. The solid is modeled as a plate of negligible thickness under the Euler-Bernoulli approximation. It is assumed that the deformation does not depend on the spanwise coordinate, so that the linearized equilibrium equation of the coupled fluid-solid system has the following expression:

$$B\frac{\partial^4 W}{\partial X^4} + \mu\frac{\partial^2 W}{\partial T^2} = \langle [P] \rangle, \qquad (1)$$

where B is the flexural rigidity per unit length in the spanwise direction of the plate and μ its surface density, $[P]$ stands for the pressure jump between each side of the plate and the angles $\langle . \rangle$ denote the mean value along the span. The surrounding fluid flows at a constant velocity U_0 in the direction X and is modeled using the potential flow approximation. The velocity potential is noted Ψ. Using the following dimensionless variables,

$$x = \frac{2Z}{H}, \ z = \frac{2Z}{H}, \ t = \frac{4TB}{\mu H^2}, \ w = \frac{2W}{H}, \qquad (2)$$

$$p = \frac{P}{\rho U^2}, \ \psi = \Psi\sqrt{\mu/B}, \qquad (3)$$

and parameters,

$$m = \frac{\rho_f H}{2\mu}, \quad u = \frac{UH}{2}\sqrt{\frac{\mu}{B}}, \quad c = \frac{2C}{H}, \quad d = \frac{2D}{H}, \quad (4)$$

equation (1) becomes,

$$\frac{\partial^4 w}{\partial x^4} + \frac{\partial^2 w}{\partial t^2} = m\langle [p] \rangle. \qquad (5)$$

In the fluid domain, the non-dimensional velocity potential satisfies the Laplace equation,

$$\Delta \psi = 0, \qquad (6)$$

with the following boundary conditions:

$$\frac{\partial \psi}{\partial z} = 0 \quad \text{for } |y| = d, \qquad (7)$$

$$\frac{\partial \psi}{\partial y} = 0 \quad \text{for } |z| = 1 + c, \qquad (8)$$

$$\frac{\partial \psi}{\partial z} = \frac{\partial w}{\partial t} + u\frac{\partial w}{\partial z} \quad \text{on the plate.} \qquad (9)$$

The pressure is then linked to the potential through the linearized unsteady Bernoulli equation,

$$p = -\frac{\partial \psi}{\partial t} - u\frac{\partial \psi}{\partial x}. \qquad (10)$$

1.2 Problem in the Fourier space
Introducing the Fourier transform in space and time $\hat{h}$ of a function $h(x,t)$,

$$\hat{h}(k, \omega) = \left(\frac{1}{2\pi}\right)^2 \int_{-\infty}^{+\infty} \int_{-\infty}^{+\infty} h(x,t)e^{i\omega t}e^{ikx}\mathrm{d}t\mathrm{d}x, \quad (11)$$

equation (5) takes the following form in the Fourier space:

$$\left[k^4 - \omega^2\right]\hat{w} = -m\langle [\hat{p}] \rangle. \qquad (12)$$

A normalized potential $\hat{\varphi} = \hat{\psi}/-i(\omega - U_R k)\hat{w}$ is then introduced. Using the unsteady Bernoulli equation (10), the pressure jump may be linked to the displacement and the normalised potential $\hat{\varphi}$,

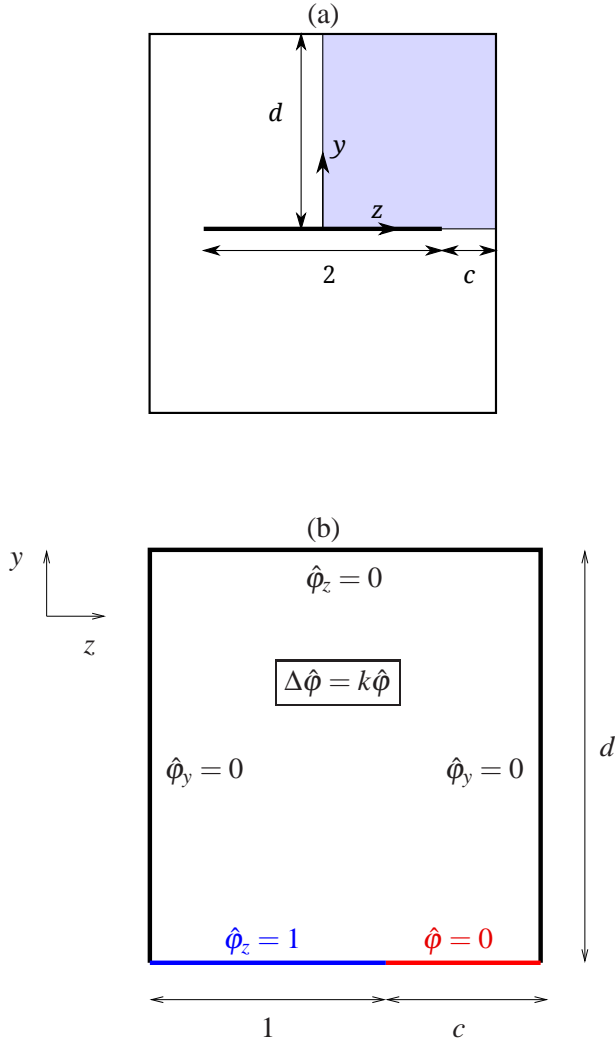$$\langle [\hat{p}] \rangle = (\omega - uk)^2\langle [\hat{\varphi}] \rangle\hat{w}. \qquad (13)$$

FIGURE 2: (a), complete geometry of the problem in Fourier space; (b), numerical domain and boundary conditions after taking into account symetries of the problem.

The Laplace equation (6) with boundary conditions (7-9) can now be expressed for the normalized velocity potential $\hat{\varphi}$. This problem is defined in the plane (y,z) of a cross-section of the plate, as sketched on Fig.2a. It can be shown that this problem is symmetric with respect to the y-axis and skew-symmetric with respect to the z-axis. Hence it can be rewritten in only one quarter of the domain as sketched on Fig.2b,

$$\frac{\partial^2 \hat{\varphi}}{\partial y^2} + \frac{\partial^2 \hat{\varphi}}{\partial z^2} = k^2 \hat{\varphi}, \quad \text{for } z \in [0, 1+c], y \in [0, d] \quad (14)$$

$$\frac{\partial \hat{\varphi}}{\partial z} = 1 \quad \text{for } z < 1, y = 0, \quad (15)$$

$$\frac{\partial \hat{\varphi}}{\partial z} = 0 \quad \text{for } y = d, \quad (16)$$

$$\frac{\partial \hat{\varphi}}{\partial y} = 0 \quad \text{for } z = 1+c \text{ and } z = 0. \quad (17)$$

This last problem depends only on k and the geometrical parameters c and d. Combining equations (12) and (13), the dispersion relation takes the following form,

$$k^4 - \omega^2 = m\frac{2g(k,c,d)}{|k|}(\omega - uk)^2, \quad (18)$$

where $g(k,c,d)$ reads,

$$g(k,c,d) = k\langle \hat{\varphi}(y=0^+)\rangle. \quad (19)$$

In the Fourier space, the work hence consists in obtaining the dispersion relation (18) for a given set of geometrical parameters. To do so, it is necessary to compute the function $g(k,c,d)$ by solving an Helmholtz problem (equation 14). The end of this section is devoted to recall the analytical form of g in various limit cases found in previous studies and present some computational results in the general case.

1.3 Limit cases for the function g found in the litterature

The different limit cases found in the litterature for the function g are presented here. The 2D limit of a plate in an infinite fluid domain is [13],

$$g = 1. \quad (20)$$

The 2D limit of a plate confined by two parallel rigid walls is [14],

$$g = \frac{1}{\tanh(kd)}. \quad (21)$$

The slender-body limit is [15],

$$g = \frac{k\pi}{4}. \quad (22)$$

Using asymptotic expansions of the 2D and slender-body limits, a composite function as been introduced to take into account the influence of a 3D flow around the plate [7],

$$g = 1 - \frac{1}{2k + \exp[(\pi/4 - 2)k]}. \quad (23)$$

In refence [8], a similar approach has been used to develop asymptotic expansions of the 2D and slender-body

limits that take into account the presence of walls perpendicular to the plate (*C* effect). A composite expansion of these two limits has then been developed, that extends the kernel of equation (23) to take into account spanwise confinement.

1.4 General case of a plate in a rectangular flow: numerical solution

In the general case of the present paper, the Helmholtz equation is solved using the open source finite element software Freefem [16] for given values of c, d and k. The resulting function g is plotted on Fig.3a for a large value of $d = 30$, and values of c in the range $[3 \times 10^{-4}, 3]$. As already reported in a previous work [8], the function g is linear at low values of k and tends to unity at large values of k. When c is large, it is correctly approximated by the infinite fluid domain 3D model [7], equation (23). Typical results when c is large are plotted on Fig.3b. Here, g is well approximated by equation (21) for large values of k while it tends to a linear slender-body type behavior at low values of k. Indeed, the function g is well fitted by a function of the form $g = Ak$ when $k \ll 1$. The value of A is plotted as function of d on Fig.4 for different values of c. When d is small, the value of A does not depend on c and the data is well fitted by,

$$A \simeq 1/3d, \quad d \ll 1. \tag{24}$$

When d is increased, A tends to a consant value which dependence on c has been characterized in a previous work [8],

$$A = \frac{k\pi}{4} \left[1 + 0.805 \ln \left(\frac{c + 0.189}{c} \right) \right]. \tag{25}$$

Now that we have the function $g(k)$, and consequently the dispersion relation, in numerical form for any combination of the numerical parameters, it will be used to compute stability boundaries of the system in two different cases: the infinite case (local instability), for which only the dispersion relation is necessary to characterize the medium, and the finite case (global instability), for which subsequent work is needed, as boundary conditions and the length have to be taken into account. In the following, numerical data will be directly used to compute the different stability limits except at low values of k, where a third order polynomial fit is used.
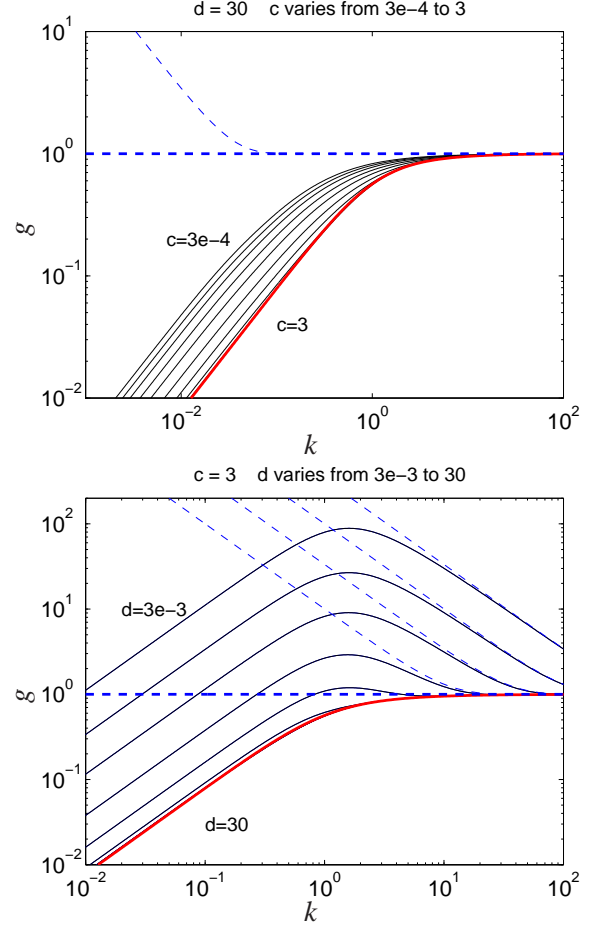

FIGURE 3: Function $g(k)$ computed numerically for various sets of the parameters c and d (solid thin lines) and compared with different limit cases; thick dashed line, equation (20); thin dashed lines, equation (21); thick solid line, equation (23).
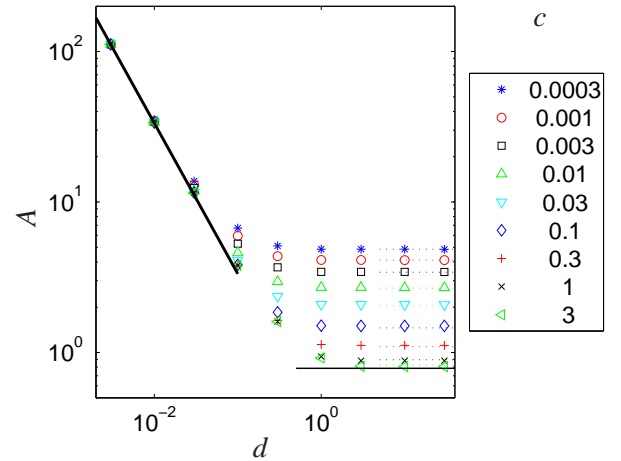

FIGURE 4: Linear coefficient of the slender-body limit (*i.e.* small wavenumbers) as function of d for different values of c. Bold line indicate the limit for low values of d, equation (24), thin line indicates the limit of unconfined flow, $A = \pi/4$ and dotted lines indicate the empirical model developed in reference [8], equation (25).
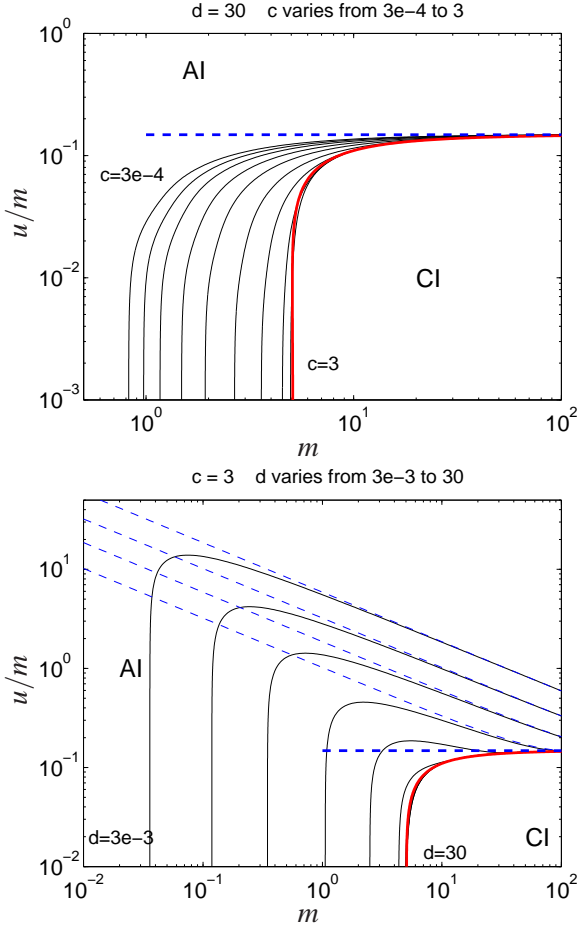
FIGURE 5: Critical curves for transition between convective and absolute instabilities (thin plain line) compared with that given by using g defined in equation (20), thick dashed line, equation (21), thin dashed lines and equation (23), thick solid line.

2 LOCAL STABILITY ANALYSIS

The instability properties of bending waves propagating in an infinite length medium in such channel flow are now studied. In its non-dimensional form, the dispersion relation depends on four parameters, the mass ratio m, the non-dimensional velocity u, the non-dimensional spanwise gap c and the non-dimensional channel height d. The dispersion relation of equation (18) is considered, where the g function is obtained by solving the Helmoltz problem (14-17), as explained in the previous section.

The temporal approach consists in solving the dispersion relation, a second order polynomial for the variable ω, associated to real values of k. If for a least one real value of k, the imaginary part of one root ω is positive, the amplitude of the associated wave $\exp[i(kx - \omega t)]$ grows exponentially with time and the medium is said locally unstable. It can be easily shown that the system bears unstable waves at any value of $u \neq 0$.

However, one may distinguish two cases of wave instability, depending on the long time impulse response of the plate. If the exponentially growing wave packet is advected by the flow, the instability is said *convective*. Conversely, if it grows in place, so that the entire space is ultimately dominated by the instability, the latter is said *absolute*. The concepts of convective and absolute instabilities, and the underlying theory, have been initially introduced in the domain of plasma physics [17] and successfully applied in the particular domain of fluid-structure interaction [13]. In the present paper, a numerical method presented in reference [18] is used to compute the critical curves for transistion between convective and absolute instabilities. The results are plotted on Fig.5 in the $(m, u/m)$ plane. On Fig.5a, $d = 30$ and c varies from 3×10^{-4} to 3. On Fig.5b, $c = 3$ and d varies from 3×10^{-3} to 30. All curves share a common limit at large values of m. This limit ($u/m = 0.148$) is that given by a 2D approach, where $g = 1$. It is actually twice the value found by Crighton & Oswell [13] in the case of a compliant panel with a flow on one side only, whereas the flow is on both sides in the present study. It has to be noted that in this context of 3D flow, the 2D limit corresponds to large values of the wavenumber. It is consistent with the fact that when $m \to \infty$, the wavenumber at which convective to absolute instability transition arises also tends to infinity.

The infinite derivative of all these curves at low values of m corresponds to the opposite limit where the wavenumber at transition is small. This is the slender body limit. In the case of a fluid-conveying pipe, which is properly described by a similar dispersion relation in the slender-body limit, Kulikoskii [19] showed that the transition does not depend on the flow velocity, but only on the mass-ratio. Again, this is consistent with the vertical limit observed on Fig.5: an added mass effect of the channel confinement modifies the mass ratio in the slender-body limit and the asymptotic value of m varies. The more the plate is confined (small c and d), the larger is the added mass. Hence the smaller is the critical value of m. Two additionnal asymptotic cases are ploted on Fig.5: the curve obtained using an analytical solution of the Helmotlz problem in a 2D case with walls (blue dotted) and the curve obtained considering the 3D flow without walls (thick red). The numerical data tends to these two limits in a consistent manner.

3 GLOBAL STABILITY ANALYSIS

When studying a finite length system during timescales such that boundaries have an influence on the dynamics,

boundary conditions must be taken into account. A plate clamped at $X = 0$ and free at $X = L$ is now considered. The problem is now rescaled using L as a characteristic length, so that the following non-dimensional variables and parameters are introduced,

$$x = \frac{X}{L}, y = \frac{Y}{L}, z = \frac{Z}{L}, w = \frac{W}{L}, t = \frac{UT}{L}, p = \frac{P}{\rho U^2}. \quad (26)$$

$$M^* = \frac{\rho L}{M}, U^* = \sqrt{\frac{M}{B}} LU, H^* = \frac{H}{L}, C^* = \frac{C}{L}, D^* = \frac{D}{L}. \quad (27)$$

In this finite length approach, the dimensionless equation of motion is now

$$\frac{\partial^2 w}{\partial t^2} + \frac{1}{U^{*2}} \frac{\partial^4 w}{\partial x^4} = M^* \langle [p] \rangle, \quad (28)$$

and the clamped-free boundary conditions are

$$w(x=0) = \frac{\partial w}{\partial x}\bigg|_{x=0} = \frac{\partial^2 w}{\partial x^2}\bigg|_{x=1} = \frac{\partial^2 w}{\partial x^2}\bigg|_{x=1} = 0 \quad (29)$$

Stability analysis is done through a modal analysis of the system. By looking for solutions of the problem in the form

$$w(x,t) = \phi(x) e^{i\omega t}, \quad (30)$$

and assuming that pressure forces exerted on the plate can be expressed as linear functions of the displacement w, one end up with a Sturm-Liouville eigenvalue problem that does not have an analytical solution in the general case. If one eigenvalue has a negative imaginary part, the system is unstable, as the temporal evolution of displacement is such that it diverges when time goes to infinity. The corresponding real part gives then the circular frequency. In practice the system has to be put in a form suitable for numerical integration. Equation (13) may be rewritten in the form,

$$\frac{k\hat{p}}{g} = (\omega - k)^2 \hat{w}. \quad (31)$$

Taking the inverse transform of this expression leads to a solution in the form of a convolution integral for the pressure,

$$\frac{1}{2\pi} \int_0^1 p'(v) G(x-v) dv = \left(\frac{\partial}{\partial t} + \frac{\partial}{\partial x} \right)^2 w, \quad (32)$$

where prime denotes for derivation with respect to the axial coordinate and $G(x)$ is the inverse Fourier transform of $1/g(k)$,

$$G(x) = \int_0^\infty \frac{\sin(kx)}{g(k)} dk. \quad (33)$$

It has to be noted that as G diverges when x tends to 0, the Cauchy's principal value of the integral in equation (32) has to be taken. As done in previous papers [7, 8], the displacement is decomposed on the modes of the plate in vacuum $\phi_i(x)$,

$$w(x,t) = e^{i\omega t} \sum_i a_i \phi_i(x). \quad (34)$$

Next, the pressure associated with the mode i is expanded on Chebyshev polynomials of the first kind and assumed to have an inverse square root singularity,

$$p_i'(x) = \sum_j A_{ij} \frac{T_j(2x-1)}{\sqrt{x(1-x)}}. \quad (35)$$

This expansion is then inserted into the integral expression for the pressure (32). A scalar product with Chebyshev polynomials of the second kind $U_k(2x-1)$ is applied. This leads to a linear problem for A_{ij}, which is solved numerically for a given set of the geometrical parameters (C^*, D^*, H^*). This method necessitates the knowledge of the function $G(x, C^*, D^*, H^*)$. In practice, it is calculated numerically using,

$$G(x) = \frac{1}{x} + G_1(x), \quad (36)$$

with,

$$G_1(x) = \int_0^\infty \sin(kx) \left(\frac{1}{g(k)} - 1 \right) dk. \quad (37)$$

As the integrand tends to zero when k tends to infinity, this integral is easily computed numerically.

Numerical results are now presented. It has to be noted that they involve a significant amount of numerical steps: Helmotlz equation using finite elements, numerical inverse Fourier transform, various projections (Chebyshev modes and Galerkin modes) and finally an eigenvalue problem.
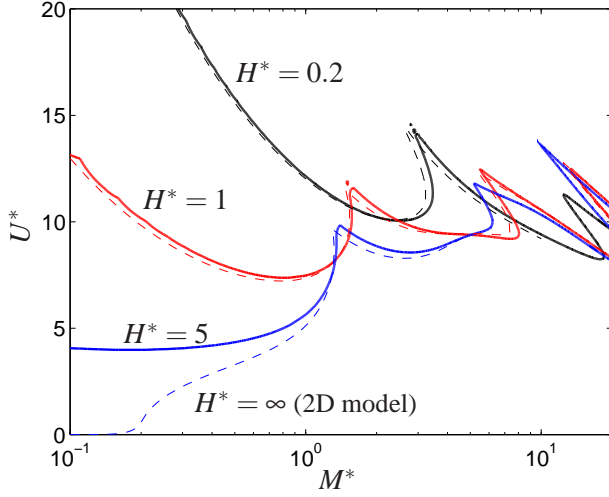
FIGURE 6: Critical curves of marginal stability at $c = 3$ and $d = 30$ obtained by the present numerical method (solid lines), compared to critical curves obtained considering an unbounded flow [7] (dashed lines).

A first set of results is presented on Fig.6. It consists in comparing the critical curves for apparition of instability in the (M^*, U^*) plane when the channel is large, $(c, d) = (3, 30)$, with that of previous studies in an unbounded flow (C^* and $D^* = \infty$). A good agreement is found between the two methods.

Another comparison is done with results of Guo and Païdoussis [14] for $D^* = 0.2$ on Fig.7a,b. Here again, the critical curves of the present 3D model tend to that predicted by a 2D model when H^* is increased. It appears that the smaller is C^*, the faster is the convergence. The main result of this comparison is that for low values of M^*, the 2D limit of reference [14], can be reached only for very large H^* or very low C^*. This is in practice difficult to achieve experimentally.

DISCUSSION

In this article, the influence of the walls of a rectangular channel on the critical velocity for flutter instability has been characterized. Local and global stability analyses have been performed. In the local approach the system is always unstable, provided the fluid is not still. Critical values of the parameters for transition between convective and absolute instabilities have been computed. In a general manner, confinement is found to significantly affect the local stability properties of the medium. Next, global stability of the finite length system has been investigated. The crucial importance of the 3D modeling at low values of the mass ratio has been emphasized. Indeed, it is found that 2D models predict the correct critical velocity
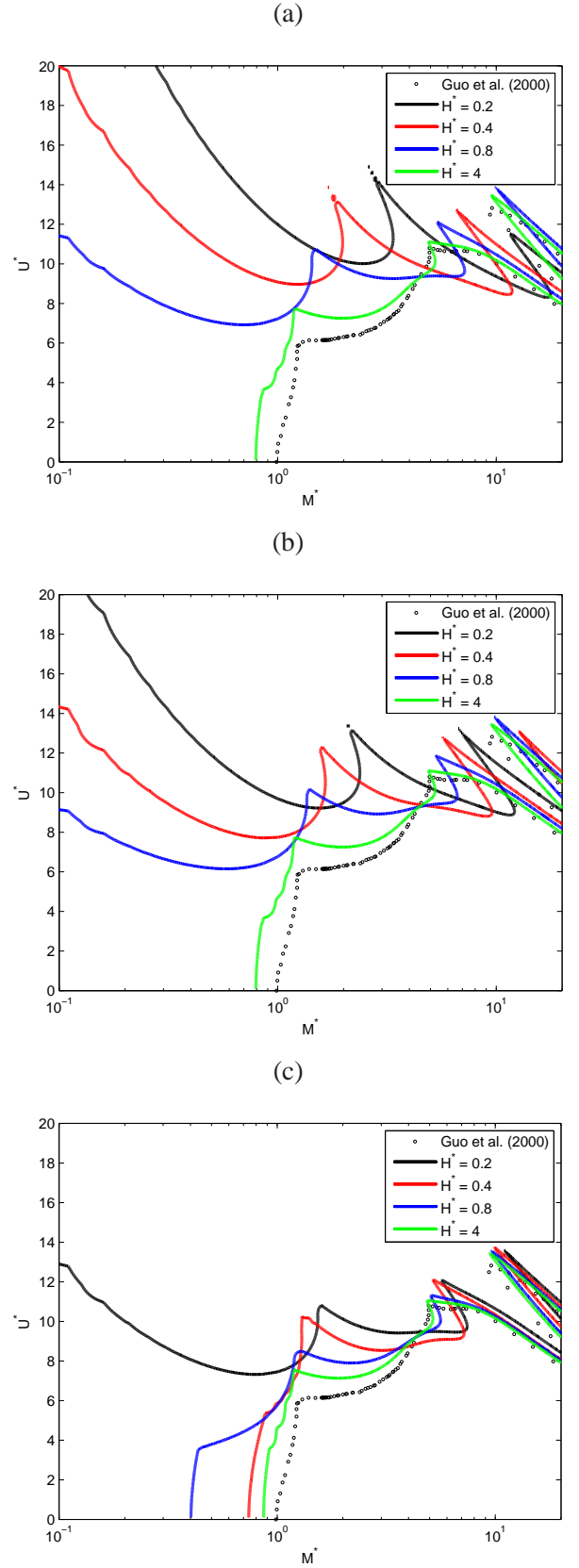

FIGURE 7: Critical curves of marginal stability at $D^* = 0.2$ for different values of H^*, compared with the 2D results of reference [14]; (a) $c = 3$, (b) $c = 0.1$, (c) $c = 0.001$. The small irregularities of the curves are due to imprecisions of the numerical method.

only for high values of the aspect ratio or low values the spanwise and lateral confinements.

When confinement is important, one may wonder if the viscosity has an effect on the instability thresholds. In the case spanwise confinement (small values of C^*), the effect of the existence of a boundary layer has been discussed in reference [12]. In this case, only the edges of the plate are affected by the presence of a boundary layer and the experimental results are found to be in good agreement with the theoretical predictions. Conversely, in the case of significant confinement by walls parallel to the plate (small values of D^*), viscosity may play a more important role. Here the whole surface may be affected by viscous drag and it may be necessary to consider a boundary layer of a Poiseuille-type flow.

Further work is now mainly focused on experiments.

REFERENCES

[1] Païdoussis, M. P., 2004. *Fluid-structure Interactions. Slender Structures and Axial Flow*, Vol. 2. Academic Press.

[2] Shelley, M. J., and Zhang, J., 2011. "Flapping and Bending Bodies Interacting with Fluid Flows". *Annual Review of Fluid Mechanics, 43*(1), pp. 449–465.

[3] Kornecki, A., Dowell, E. H., and O'Brien, J., 1976. "On the aeroelastic instability of two-dimensional panels in uniform incompressible flow". *Journal of Sound and Vibration, 47*(2), pp. 163–178.

[4] Huang, L., 1995. "Flutter of cantilevered plates in axial flow". *Journal of Fluids and Structures, 9*(2), pp. 127–147.

[5] Aurégan, Y., and Depollier, C., 1995. "Snoring: Linear stability and in-vitro experiments". *Journal of Sound and Vibration, 188*(1), pp. 39–53.

[6] Lemaitre, C., Hémon, P., and de Langre, E., 2005. "Instability of a long ribbon hanging in axial air flow". *Journal of Fluids and Structures, 20*(7), pp. 913–925.

[7] Eloy, C., Souilliez, C., and Schouveiler, L., 2007. "Flutter of a rectangular plate". *Journal of Fluids and Structures, 23*(6), pp. 904–919.

[8] Doaré, O., Sauzade, M., and Eloy, C., 2011. "Flutter of an elastic plate in a channel flow: Confinement and finite-size effects". *Journal of Fluids and Structures, 27*(1), pp. 76–88.

[9] Taneda, S., 1968. "Waving motions of flags". *Journal of the Physical Society of Japan, 24*(2), pp. 392–401.

[10] Datta, S., and Gottenberg, W., 1975. "Instability of an elastic strip hanging in an airstream". *Journal of Applied Mechanics, 42*, pp. 195–198.

[11] Eloy, C., Kofman, N., and Schouveiler, L., 2012. "The origin of hysteresis in the flag instability". *Journal of Fluid Mechanics, **In press***.

[12] Doaré, O., Mano, D., and Bilbao Ludena, J. C., 2011. "Effect of spanwise confinement on flag flutter: Experimental measurements". *Physics of Fluids, 23*, p. 111704.

[13] Crighton, D., and Oswell, J. E., 1991. "Fluid loading with mean flow. I. Response of an elastic plate to localized excitation". *Philosophical Transactions of the Royal Society of London A, 335*, pp. 557–592.

[14] Guo, C. Q., and Paidoussis, M. P., 2000. "Stability of Rectangular Plates With Free Side-Edges in Two-Dimensional Inviscid Channel Flow". *Journal of Applied Mechanics, 67*(1), pp. 171–176.

[15] Lighthill, M., 1960. "Note on the swimming of slender fish". *Journal of FLuid Mechanics, 9*(2), pp. 305–317.

[16] Hecht, F., and le Hyaric, A. http://www.freefem.org/ff++/index.htm.

[17] Briggs, R. J., 1964. *Electron-Stream Interaction with Plasmas*. The MIT Press.

[18] de Langre, E., 2002. "Absolutely unstable waves in inviscid hydroelastic systems". *Journal of Sound and Vibration, 256*(2), pp. 299–317.

[19] Kulikovskii, A. G., and Shikina, I. S., 1988. "On the bending oscillations of a long tube filled with moving fluid". *Izv. Akad. Nauk. ArmSSR, Mekhanika, 41*(1), pp. 31–39.